ASME Journal of Solar Energy Engineering
Online journal at:
https://asmedigitalcollection.asme.org/solarenergyengineering

Thermodynamic Performance Investigation of Environmentally Friendly Working Fluids in a Geothermal Integrated Pumped Thermal Energy Storage System

Aggrey Mwesigye
Department of Mechanical and Manufacturing Engineering,
Schulich School of Engineering,
University of Calgary,
Calgary, AB T2N 1N4, Canada
e-mail: aggrey.mwesigye@ucalgary.ca

Among the available energy storage technologies, pumped thermal energy storage (PTES) is emerging as a potential solution for large-scale electrical energy storage with high round-trip efficiencies and no geographical limitations. However, PTES requires a low-cost, high-temperature heat source to achieve reasonable round-trip efficiencies. Moreover, organic Rankine cycle-based PTES systems require high-performance and environmentally friendly working fluids. In this study, the thermodynamic performance of a geothermal integrated PTES system using environmentally friendly working fluids is investigated. The mathematical model of the geothermal integrated PTES system is developed using the first and second laws of thermodynamics and implemented in Engineering Equation Solver (EES). With the developed model, the thermodynamic performance of the PTES system for different working fluids, including butene, cyclopentane, isobutene, R1233zd(E), R1234ze(Z), R1224yd(Z), HFO1336mzz(Z), n-hexane, and n-pentane was investigated. For geothermal fluid outlet temperatures between 60 °C and 120 °C and geothermal fluid inlet and outlet temperature differences across the evaporator between 20 °C and 60 °C, the net power ratio, i.e., the ratio of the electrical energy discharged to the electrical energy used to run the charging cycle, is between 0.25 and 1.40. This shows that the system has the potential to give back more than 100% of the electrical energy used during charging under certain conditions. High net power ratios are obtained for a combination of high source temperatures and low geothermal fluid inlet and outlet temperature differences.
[DOI: 10.1115/1.4065554]

Keywords: energy storage, exergetic efficiency, geothermal energy, net power ratio, pumped thermal energy storage, exergy, renewable energy, thermodynamic performance

1 Introduction

The increasing concerns about climate change and the urgent need to diversify our energy use and generation systems have increased the search, development, and deployment of clean and renewable energy technologies. However, most renewable energy resources are intermittent, available when the demand is low and not available when required. As such, energy storage is increasingly becoming an important part of our transition to net-zero emissions. Importantly, energy storage helps address the mismatch between demand and supply, thereby facilitating the penetration of renewable energy in the electric grid.

For large-scale energy storage, the pumped hydro energy storage technology accounts for over 96% of the available large-scale energy storage systems [1,2]. Compressed air energy storage (CAES) is another technology available for large-scale energy storage. These commercially developed energy storage technologies have geographical limitations requiring the presence of a large water body for pumped hydro or salt caverns for compressed air energy storage systems [2]. As such, current research in large-scale energy storage is looking at addressing these challenges by developing technology with high round-trip efficiencies and no geographical limitations. Among the emerging energy storage technologies, pumped thermal energy storage (PTES) and liquid air energy storage (LAES) systems are gaining increasing research interest since they use available components (such as turbines, compressors, pumps etc.) and are not limited by geography [3]. Of the two, PTES systems stand out as a potential solution for large-scale energy storage without geographical limitations and higher round-trip efficiencies [4]. Round-trip efficiencies as high as 125% have been predicted in several theoretical studies [4].

Pumped thermal energy storage or compressed heat energy storage (CHEST) systems are part of the Carnot battery energy storage technology [3,5]. Rankine cycle PTES systems consist of a charging cycle driven by a high-temperature heat pump using

Contributed by the Solar Energy Division of ASME for publication in the Journal of Solar Energy Engineering: Including Wind Energy and Building Energy Conservation. Manuscript received September 29, 2023; final manuscript received May 5, 2024; published online June 13, 2024. Assoc. Editor: Justin Lapp.

excess electricity and a discharging cycle generating electricity during peak hours as needed. Brayton cycle-based PTES systems are also increasingly being considered; however, they require much higher temperatures for the same efficiency levels as Rankine cycle-based systems [5]. These systems are the subject of increasing research studies aimed at understanding and optimizing their performance under different operating conditions.

Among the reasons for higher round-trip efficiencies in PTES systems is the use of higher heat pump evaporator temperatures. With higher evaporator temperatures, the power required to drive the heat pump's compressor during the charging cycle is lower than the power released during the discharging cycle. Moreover, the temperature difference between the high-temperature storage and the heat sink for the organic Rankine cycle is higher, resulting in higher electricity generation than that used by the heat pump during charging.

Parisi et al. [6] investigated different cycle configurations using reversible turbomachinery for pumped thermal energy storage. They considered both the Brayton cycle with different working fluids and the subcritical Rankine cycle using ammonia as the working fluid. Steinmann et al. [4] considered a PTES system for smart sector-coupling of heat and electricity. They showed that for a heat source temperature of 100 °C and a sink temperature of 15 °C, a net power ratio of 1.25 can be achieved. The net power ratio is the ratio of the electrical energy discharged from storage to the electrical energy used for charging the system. In their study, source and sink temperatures are assumed to stay constant. Jockenhöfer et al. [7] considered a pumped thermal energy storage system with low-temperature heat integration. They also showed a net power ratio of up to 1.25.

Frate et al. [8] showed that thermal integration in a PTES system increased the round-trip efficiency above 100%. For source temperatures between 80 °C and 110 °C, the maximum round-trip efficiency was 1.3 or 130% with R1233zd(E) as a working fluid. In a recent study, Frate et al. [9] investigated the performance of a solar thermally integrated PTES. They showed round-trip efficiencies between 0.85 and 0.87. Weitzer et al. [10] considered open flash cycles in Rankine cycle-powered PTES with large storage temperature spreads. The source temperatures were 30–90 °C, and a storage temperature of 150 °C was considered. Pressurized water was used as the storage medium.

Other studies have demonstrated significantly lower round-trip efficiencies for PTES systems. Tian et al. [11] showed that for different organic Rankine power cycles used in a PTES system, the maximum round-trip efficiency was 31.15%, and the maximum exergetic efficiency was 23.40%. They considered R245fa as the working fluid. However, R245fa has a global warming potential of 950. Steger et al. [12] designed a reversible heat pump—organic Rankine cycle pilot plant for energy storage with a target round-trip efficiency of 59%. The source temperature was 90 °C, and R1233zd(E) was used as the working fluid. Performance with cyclopentane, R123, and R365 was also briefly discussed.

The role of the thermal energy storage medium in the overall system performance is an important consideration in designing PTES systems. Zhao et al. [13] recently investigated thermal energy stores for PTES systems. They showed that round-trip efficiencies between 62% and 100% could be achieved, indicating the influence of the type of thermal energy storage on system performance. A comparison of latent and sensible thermal energy storage in a PTES was presented by Eppinger et al. [14]. For a 20-kW demonstration plant, they showed power-to-power efficiencies of 80% when latent thermal energy storage was used compared to 62% with sensible thermal energy storage.

Different sources of the high temperatures required by the heat pump have been investigated, ranging from solar [9,15], waste heat [3], and high-temperature steam [16], among others. One other potential source is geothermal, especially low-temperature geothermal, which might not be suitable for direct electrical generation. The integration of geothermal with pumped thermal energy storage has not been widely investigated. Moreover, there is potential for coupling PTES systems with depleted or abandoned oil and gas wells, offsetting the cost that would be required to drill new wells for PTES geothermal integration [17–19].

From the reviewed studies, there is increasing interest in PTES systems for energy storage. Available literature shows that the performance of PTES systems is significantly dependent on the operating conditions, especially the source and storage temperatures and the working fluid used. In addition, with the impending phasing out of refrigerants with high global warming potentials, the performance of newly developed refrigerants in energy systems is essential. In this study, a geothermal integrated pumped thermal energy system using nine environmentally friendly working fluids is investigated. The considered refrigerants are Butene, cyclopentane, HFO1336mzz(Z), isobutene, R1233zd(E), R1234ze(Z), R1224yd(Z), n-hexane, and n-pentane. Furthermore, a geothermal heat source with a range of temperatures between 60 °C and 130 °C representing the possible temperatures from conventional geothermal resources and temperatures obtainable from depleted oil wells is considered. The storage temperature is kept low such that low enthalpy geothermal resources can be investigated. As such, a melting temperature of 133 °C was used in this study.

2 Physical Model

Figure 1 shows the schematic of a PTES system and its integration with a geothermal source through a co-axial heat exchanger. The hot geothermal fluid from the borehole heat exchanger enters the heat pump's evaporator with a temperature T_{in} and exchanges heat with the refrigerant in the heat pump cycle, causing the temperature to drop. The geothermal fluid at a lower temperature returns to the borehole heat exchanger at a temperature T_{out} and collects more energy for the next cycle.

The refrigerant that has gained energy from the geothermal fluid exits the evaporator at state 1 and is compressed to a high pressure and, thus, a temperature higher than the melting temperature of the phase change material (PCM) in the thermal energy storage tank. The refrigerant from the compressor rejects heat to the energy storage material, condenses, and expands through an expansion valve to the pressure of the evaporator. The charging of the PTES is done using cheap excess electricity during off-peak hours. When there is a high demand for energy during peak hours, the organic Rankine cycle of the discharging cycle is turned on, absorbing energy from the thermal storage tank. Thus, the boiling temperature of the working fluid in the organic Rankine cycle is set to a temperature lower than the melting temperature of the PCM used for thermal energy storage. Two configurations of the PTES system are shown in Fig. 1: (a) without recuperation and (b) with recuperation using an internal heat exchanger.

For the geothermal system, a concentric borehole heat exchanger is considered, as shown in Fig. 1. It should be noted that this heat exchanger is not modeled directly in this study. From the results of Alimonti et al. [19] using a concentric heat exchanger of 121.7 mm outer diameter and 77.9 mm inner diameter and flowrates between 8 and 20 m^3/h, heat exchanger outlet temperatures between 80 and 120 °C were obtained for a 6.1 km deep borehole. The power cycle outlet temperature, which is the inlet temperature into the borehole, was 40 °C. In this study, we have assumed geothermal source temperatures/inlet into the evaporator (T_{in}) between 60 °C and 130 °C. The difference in the geothermal fluid's inlet and outlet temperatures as it exchanges energy with the refrigerant in the evaporator is also varied between 20 °C and 60 °C, close to 40 °C and 80 °C in the Alimonti et al. [19] study. However, to ensure high values of the net power ratio, it is essential to keep the source temperatures for the heat pump as high as possible. This means allowing a smaller temperature change between the inlet and outlet of the hot stream from the borehole heat exchanger to the heat pump.

During charging, this study assumes that 1 MW of electricity is drawn from the grid by the heat pump, upgraded, and stored. The charging time is fixed at 6 h. During discharging, 1 MW of

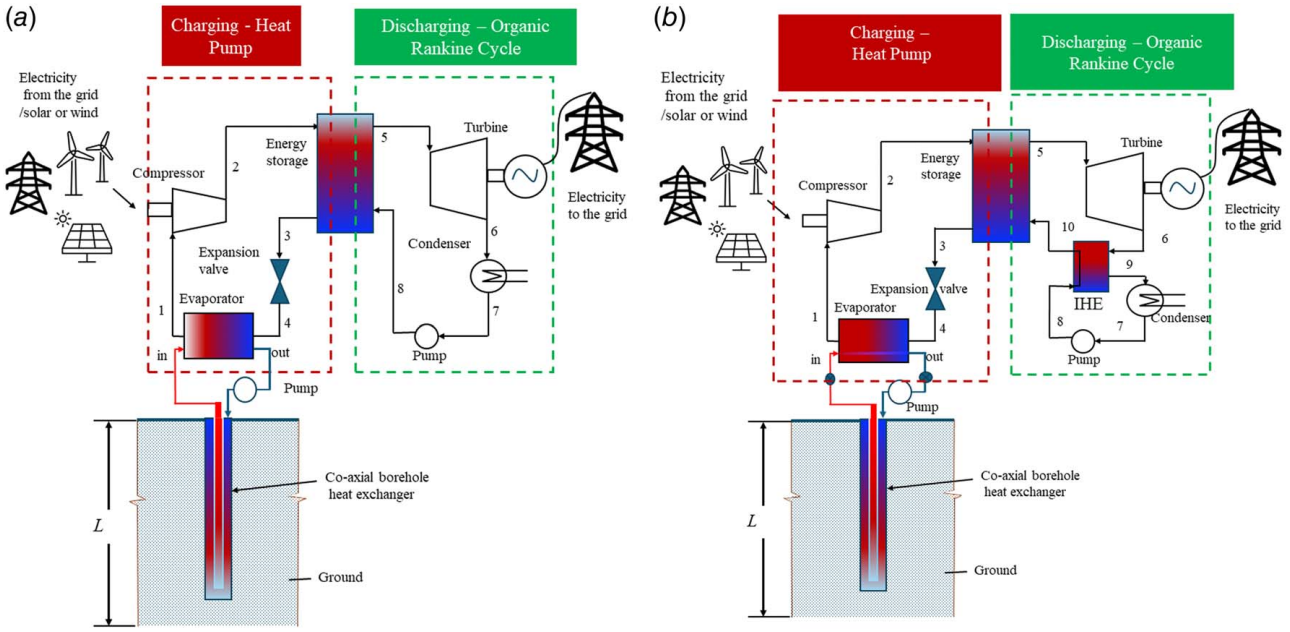

Fig. 1 Geothermal integrated PTES system (*a*) without an internal heat exchanger (IHE) and (*b*) with an internal heat exchanger

electrical energy is generated by the power cycle. Given that the energy stored is higher than the electrical energy used to run the compressor, with part of this coming from the geothermal borehole, the discharge time varies, as discussed later.

3 Materials

The thermal energy storage tank is filled with a phase change material to take advantage of the constant melting temperatures and a substantial amount of energy stored during the phase change process. For these reasons, latent thermal energy storage is desired. Besides, a comparison of sensible and latent heat storage systems for PTES showed latent heat storage to be superior to sensible heat storage [14]. In this study, a high-temperature PCM from PlusICE, A133 [20] was used in the analysis. For A133, the melting temperature is 133 °C, the latent heat is 200 kJ/kg, and the density and specific heat capacity for both the solid and liquid phases are 880 kg/m^3 and 2.2 kJ/kg °C [20], respectively. The working fluids for the heat pump and organic Rankine cycle are chosen to work for the range of melting temperatures considered. Discharge temperatures of about 120 °C were considered for the Organic Rankine cycle to ensure efficient operation. As such, the critical temperatures of the working fluids used in the heat pump and organic Rankine cycle should be greater than 120 °C. In addition, there are increasing concerns about climate change due to global warming and the need to keep the global temperature rise below 1.5 °C if we are to avoid catastrophic consequences of climate change. As such, stringent emission reduction targets are being implemented worldwide, and highly polluting substances are being phased out [21]. For this reason, working fluids with a global warming potential below 150 and no ozone depletion potential were considered. Table 1 shows the considered refrigerants and some of the important properties. These working fluids were selected from the real fluids database in Engineering Equation Solver (EES). Besides, to avoid compression in the two-phase liquid–vapor mixture, fluids with a dry or a slight isentropic curve were considered.

4 Thermodynamic Analysis

The thermodynamic model governing the performance of the geothermal integrated PTES system shown in Fig. 1 was obtained from the laws of thermodynamics. The analysis assumes steady operating conditions and negligible kinetic and potential energy changes. Further assumptions made for each component are detailed, along with the equations representing each component. The *T-s* diagram corresponding to the non-recuperated organic Rankine cycle in Fig. 1(*a*) is shown in Fig. 2.

Table 1 Properties of working fluids

Working fluid	$T_{critical}$ (°C)	h_{fg} at 133 °C (kJ/kg)	GWP	ODP	Safety
Butene	146.1	151.5	<1	0	A-3
Cyclopentane	238.6	313.2	<0.1	0	A-3
HFO1336mzz(Z)	171.3	104.6	1	0	A-1
Isobutene	144.9	145.3	3	0	A-3
R1233zd(E) [22]	165.6	108.0	4.5	0	A-1
R1234ze(Z)	150.1	94.4	1	0	A-2L
R1224yd(Z)	155.5	82.0	<1	0	A-1
n-hexane	234.7	279.1	<1	0	A-3
n-pentane	196.5	252.2	<1	0	A-3

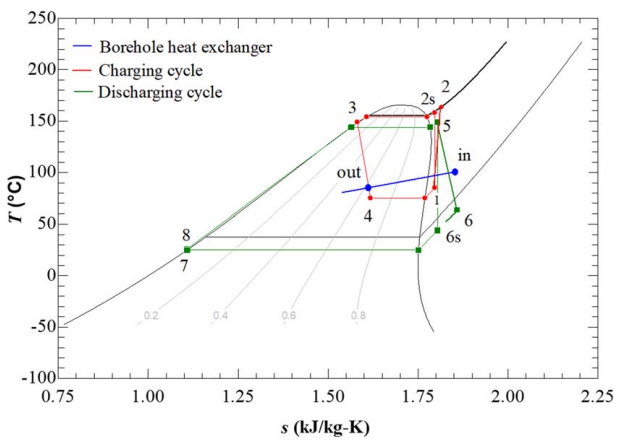

Fig. 2 Property diagram representing the non-recuperated PTES system

For the control volume around the evaporator of the heat pump in the charging cycle, an energy balance gives

$$\dot{m}_w \cdot c_{pw}(T_{in} - T_{out}) = \dot{m}_{r,c}(h_1 - h_4) \quad (1)$$

The second law analysis gives the irreversibilities in the evaporator as

$$\dot{I}_{ev} = T_o \dot{S}_{gen,ev} \quad (2)$$

where T_o is the dead state temperature taken as 298 K. An entropy balance of the control volume enclosing the evaporator gives

$$\dot{S}_{gen,ev} = \dot{m}_{r,c}(s_1 - s_4) + \dot{m}_w c_{pw} \ln\left(\frac{T_{out}}{T_{in}}\right) \quad (3)$$

For the compressor driving the charging cycle, the first law of thermodynamics with negligible heat losses gives

$$\dot{W}_c = \dot{m}_{r,c}(h_2 - h_1) \quad (4)$$

The compressor isentropic efficiency is used to obtain the actual enthalpy h_2 as $\eta_c = (h_{2s} - h_1)/(h_2 - h_1)$. h_2s is the enthalpy at $s_1 = s_{2s}$. From the entropy balance across the compressor, the exergy destruction rate for the compressor is

$$\dot{I}_c = T_o \, \dot{m}_{r,c} \, (s_2 - s_1) \quad (5)$$

For the thermal energy storage tank, the total energy stored during the charging cycle, assuming the complete melting of the phase change material, is

$$Q_s = m_s \cdot L + m_s c_{ps} \, (T_f - T_i) \quad (6)$$

where m_s is the mass of the material in the tank, L is the latent heat of the material, c_{ps} is the specific heat capacity, and T_i and T_f represent the initial and final temperatures of the thermal store, respectively. During charging, the energy transfer rate to the storage tank is

$$\dot{Q}_{23} = \dot{m}_{r,c} \, (h_2 - h_3) \quad (7)$$

To fully charge the thermal energy storage tank of mass m_s,

$$\Delta t_c = \frac{m_s \cdot L + m_s c_{ps} \, (T_f - T_i)}{\dot{m}_{r,c} \, (h_2 - h_3)} \quad (8)$$

The irreversibilities in the thermal energy storage tank during charging and assuming a perfectly insulated tank are

$$\dot{I}_{sto,c} = T_o \, \dot{m}_{r,c} \, (s_3 - s_2) \quad (9)$$

The refrigerant leaving the thermal energy storage tank/condenser is throttled through an expansion valve, with $h_3 = h_4$ and exergy destruction of

$$\dot{I}_{exp} = T_o \, \dot{m}_{r,c} \, (s_4 - s_3) \quad (10)$$

When needed, the stored energy is extracted by either running a basic organic Rankine cycle or a recuperated organic Rankine cycle, as shown in Figs. 1(*a*) and 1(*b*). The energy extracted during the discharge cycle is given by

$$\dot{Q}_{58} = \dot{m}_{r,d} \, (h_5 - h_8) \quad (11)$$

The irreversibilities during discharging of the thermal energy storage tank, assuming no other losses are given by

$$\dot{I}_{sto,d} = T_o \, \dot{m}_{r,d} \, (s_5 - s_8) \quad (12)$$

The power output of the turbine during the discharging cycle is

$$\dot{W}_t = \dot{m}_{r,d} \, (h_5 - h_6) \quad (13)$$

where the isentropic efficiency of the turbine is $\eta_c = (h_5 - h_6)/(h_5 - h_{6s})$. h_{6s} is evaluated at $s_5 = s_6$. The irreversibilities in the turbine are given by

$$\dot{I}_{turb} = T_o \, \dot{m}_{r,d} \, (s_6 - s_5) \quad (14)$$

For the condenser in the non-recuperated organic Rankine cycle in Fig. 1(*a*), the heat transfer rate is,

$$\dot{Q}_{out} = \dot{m}_{r,d} \, (h_6 - h_7) \quad (15)$$

The irreversibilities in the condenser are given by

$$\dot{I}_{cond} = T_o \left(\dot{m}_{r,d} \, (s_7 - s_6) + \frac{\dot{Q}_{out}}{T_{surr}}\right) \quad (16)$$

For the pump in the non-recuperated organic Rankine cycle, reversible work is given by

$$\dot{W}_{p,rev} = m_{r,d} \, (h_8 - h_7) = v_7 \, (p_8 - p_7) \quad (17)$$

where v_7 is the specific volume at the inlet. The actual pump work is determined from the pump's isentropic efficiency as

$$\eta_{p,is} = \frac{\dot{W}_{p,rev}}{\dot{W}_p} \quad (18)$$

The irreversibilities for the pump are given by

$$\dot{I}_p = T_o \, \dot{m}_{r,d} \, (s_8 - s_7) \quad (19)$$

Since the charging and discharging processes can take place independently, the irreversibilities during charging and discharging are summed up separately, such that for the charging cycle, the total irreversibilities are

$$\dot{I}_{total,c} = \dot{I}_{ev} + \dot{I}_c + \dot{I}_{sto,c} + \dot{I}_{exp} \quad (20)$$

and for the discharging cycle, the total irreversibilities are

$$\dot{I}_{total,d} = \dot{I}_t + \dot{I}_{sto,d} + \dot{I}_{cond} + \dot{I}_p \quad (21)$$

The thermal efficiency of the organic Ranking cycle during the discharging cycle is given by

$$\eta_{th} = \frac{\dot{W}_t - \dot{W}_p}{\dot{Q}_{58}} \quad (22)$$

The second law of efficiency of the Organic Rankine cycle during discharging is given by

$$\eta_{II} = \frac{\eta_{th}}{\left(1 - \frac{T_{sink}}{T_m}\right)} \quad (23)$$

where T_{sink} and T_m are the lowest (sink) and source temperatures of the discharging cycle, respectively. T_m is the temperature of the storage medium where the heat exchanger carrying the working fluid circulating in the organic Rankine cycle is embedded. The second law of efficiency of the heat pump cycle during charging is

$$\eta_{II,c} = \frac{\text{COP}}{\text{COP}_c} \quad (24)$$

The coefficient of performance (COP) of a Carnot cycle for a heat pump is $\text{COP}_c = T_2(T_2—T_4)$, and the coefficient of performance of the actual cycle is $\text{COP} = \dot{Q}_{23}/\dot{W}_c$. Where T_4 and T_2 are taken as the lowest and highest temperatures of the charging cycle, respectively, according to the *T-s* diagram in Fig. 2.

To determine the effectiveness of the entire PTES system, a net power ratio is defined as the ratio of the electrical energy discharged by the organic Rankine cycle to the electrical energy used during the charging of the system (compressor and pumping of the geothermal fluid) as

$$\phi = \frac{(\dot{W}_t - \dot{W}_p)\Delta t_d}{\dot{W}_c \Delta t_c} \quad (25)$$

The compressor power input is taken to be the same as the discharge power output. As such, the discharge time is given by

$$\Delta t_d = \frac{m_s L + m_s c_{ps}(T_f - T_i)}{\dot{m}_{r,d}(h_5 - h_8)} \tag{26}$$

For the recuperated organic Rankine cycle with an internal heat exchanger, an energy balance gives

$$\dot{m}_{r,d}\,(h_{10} - h_8) = \dot{m}_{r,d}\,(h_6 - h_9) \tag{27}$$

The heat exchange between the different streams is given by

$$\dot{Q}_{IHE} = \varepsilon \dot{m}_{r,d}\, c_{p,min}\,(T_6 - T_8) \tag{28}$$

where ε is the heat exchanger effectiveness and $c_{p,min}$ is the minimum specific heat capacity of the two streams. The effectiveness is set to 0.95 in this study. With recuperation, less energy will be drawn from the energy storage for the same power output, increasing the efficiency of the cycle and increasing the discharge time, according to Eq. (26).

5 Solution Procedure

Equations (1)–(28) are exact, requiring only the thermodynamic property data for the solution to be obtained. In this study, the equations representing the thermodynamic model of the system were implemented in EES [23]. The thermodynamic properties at each state are obtained from the built-in thermodynamic property data. The thermodynamic states corresponding to the point labels in Fig. 1(*a*) are shown on the *T-s* diagram in Fig. 2. The *T-s* diagram is a means of validating the processes taking place during charging and discharging cycles as well as a means of visualizing these processes. For the pressures used, the *T-s* diagram shows the charging process, starting with a superheated vapor into the compressor at 1, compression to 2, condensation to 3 as the heat is stored, throttling through an expansion device to 4, and evaporation as the refrigerant goes through the evaporator/heat exchanger connecting the heat pump cycle with the geothermal borehole heat exchanger to 1. The non-recuperated discharging cycle involves heat extraction from storage from 8 to 5, expansion in a turbine 5 to 6, condensation 6 to 7, and pumping 7 to 8 back to the pressure of the turbine inlet. In this analysis, the melting temperature of the material in the thermal energy storage tank is kept constant since a specific phase change material was specified. The power output of the turbine is taken to be the same as the power used to charge the system, i.e., power input to the compressor. The simulation parameters used in this study are shown in Table 2.

Although the compressor work is fixed at 1 MW in this study, changing the heat source's mass flowrate will change the output. For example, if a 2 MW input was the energy to be stored, the borehole heat exchanger mass flowrate would be doubled, or two borehole heat exchangers would be required.

Table 2 Simulation parameters used in the study

Compressor isentropic efficiency, η_c	90%
Turbine isentropic efficiency, η_t	90%
Storage temperature, T_m (°C)	133
Borehole heat exchanger outlet temperature, T_{out} also called T_{source} (°C)	60–120
Borehole heat exchanger inlet temperature, T_{in} (°C)	$T_{in}-\Delta T_o$
ΔT_o (°C)	10–60
Sink temperature, T_{sink} (°C)	15–35
Compressor superheat, T_{sup} (°C)	15
Pinch point temperature for heat exchangers (°C)	5
Compressor power input, (MW)	1.0
Turbine power output, (MW)	1.0
Dead state temperature, T_o (°C)	25
Heat pump condensing temperature (°C)	T_m+5
ORC boiling temperature (°C)	T_m-5
Storage efficiency	100
Δt_c (hours)	6.0

6 Results and Discussion

The net power ratio, defined as the ratio of the electrical energy discharged by the power cycle to the electrical energy input into the charging cycle, is an important parameter for characterizing the performance of PTES systems. It is comparable to the round-trip efficiency used to characterize energy storage systems. Because this value can be greater than 1, it is preferably called the net power ratio. Values greater than 1 mean the electrical energy discharged is greater than the electrical energy input used for charging the system. Figure 3 shows the variation of the net power ratio with source temperature for different working fluids. This graph is obtained for the parameters shown in Table 2, a geothermal fluid inlet and outlet temperature difference of $\Delta T_o = 20$ °C, a sink temperature of $T_{sink} = 20$ °C, a compressor power input of 1 MW, and a turbine power output of 1 MW. As the figure shows, the net power ratio increases as the source temperature increases for each working fluid. This is expected since an increase in the source temperature for the charging cycle means less compressor work input and, thus, a higher heat pump COP.

Figure 3 also shows that of the considered working fluids, cyclopentane gives the highest performance, followed by n-hexane and n-pentane for the melting temperature used in this study. This is likely related to the higher latent heat of vaporization of these refrigerants at the considered melting temperature. The value of the melting temperature is way below the critical temperatures of these working fluids, as shown in Table 1. Moreover, Fig. 3 shows the existence of conditions for which the net power ratio is greater than 1. That is, we get more electrical energy during the discharge cycle than the electrical energy used during the charging period. This is possible because, at high temperatures, additional thermal energy from the geothermal resource is used to complement the electrical energy input into the compressor.

Another important parameter that affects the performance of the PTES system is the COP of the high-temperature heat pump used for the charging cycle. For the PTES system, it is defined as the ratio of the energy transferred to the storage medium through the condenser to the compressor work input. Figure 4 shows the variation of the COP as a function of source temperature for the different working fluids. The COP increases as the source temperature increases, as expected. At higher source temperatures, more thermal energy from the geothermal source is available. Thus, less compressor power is used. Similar to the net power ratio, cyclopentane shows the highest COP of the considered working fluids.

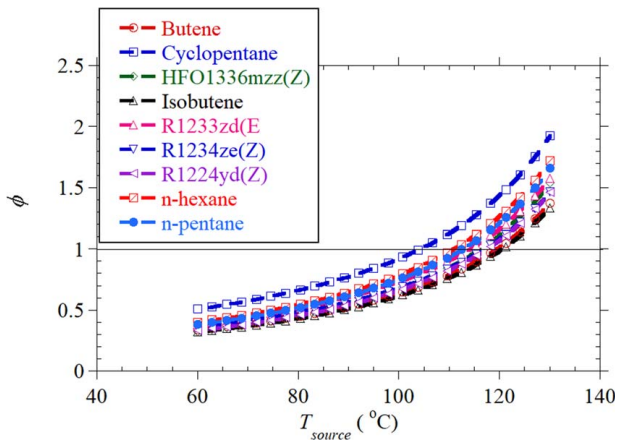

Fig. 3 Net power ratio as a function of source temperature for different working fluids with $\Delta T_o = 20$ °C and $T_{sink} = 20$ °C for a 1-MW system

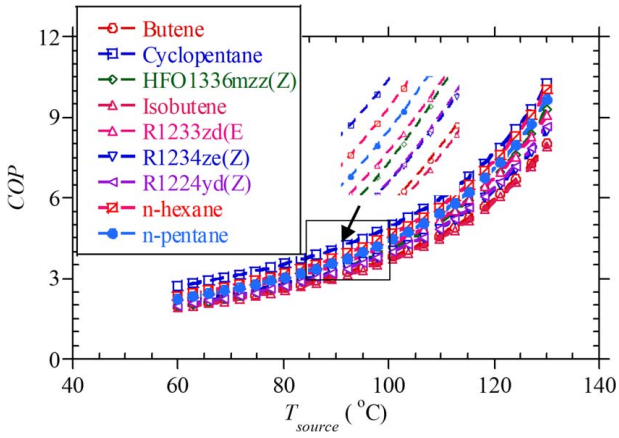

Fig. 4 COP as a function of source temperature for different working fluids with $\Delta T_o = 20$ °C and $T_{sink} = 20$ °C for a 1-MW system

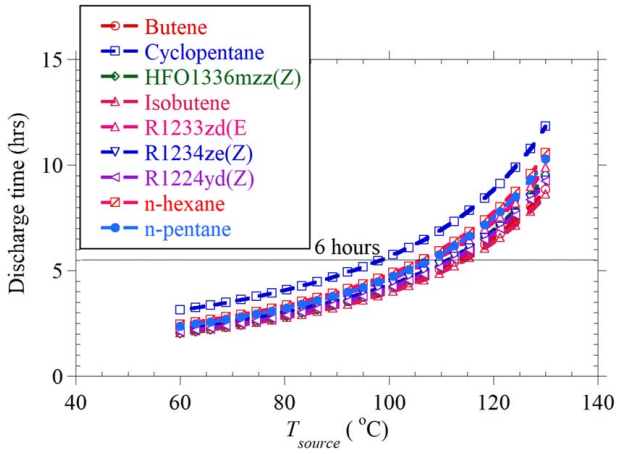

Fig. 6 Discharge time as a function of source temperature for different working fluids with $\Delta T_o = 20$ °C and $T_{sink} = 20$ °C for a 1-MW system

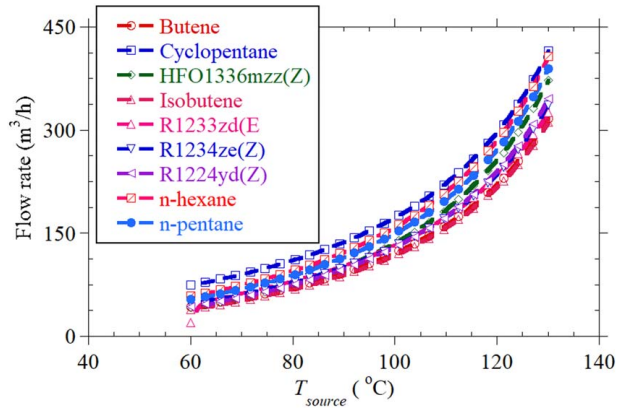

Fig. 5 Borehole heat exchanger flowrate as a function of source temperature with $\Delta T_o = 20$ °C and $T_{sink} = 20$ °C for a 1-MW system

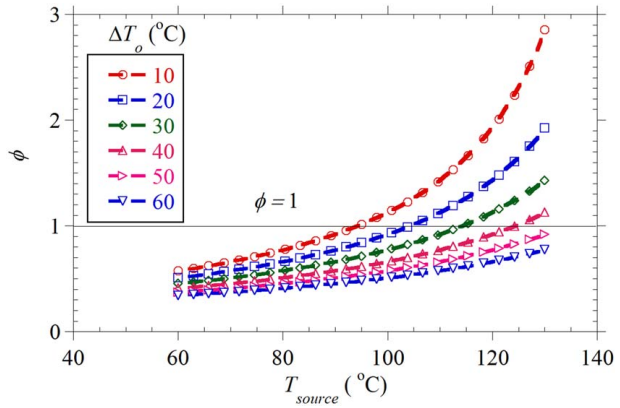

Fig. 7 Net power ratio as a function of source temperature and geothermal fluid inlet and outlet temperature difference (ΔT_o) for cyclopentane with $T_{sink} = 20$ °C and a 1-MW system

Although the working fluids with higher values of the latent heat of vaporization at the considered melting temperature show better performance, for the fixed power input, the flowrate required from the geothermal source will be higher. Figure 5 shows the variation of the required volume flowrate from the geothermal source as a function of source temperature. For the considered 1 MW charging and discharging rate, a 20 °C temperature difference between the inlet and outlet of the geothermal fluid, flowrates between 40 and 420 m^3/h are required depending on the working fluid considered. Cyclopentane, n-hexane, and n-pentane, in that order, require higher flowrates at a given source temperature. This is in line with Eq. (1) since the refrigeration flowrate is fixed by the compressor's power input, the larger enthalpy difference between states 1 and 4 requires a larger geothermal fluid mass flowrate. Furthermore, increasing the source temperature means a larger heat transfer rate into the evaporator. This requires a corresponding increase in the mass flowrate from the geothermal heat source for the fixed temperature difference of the inlet and exit geothermal streams (ΔT_o), in this case, $\Delta T_o = 20$ °C for the results presented in Fig. 5.

Because the charging power input and discharging power output are the same, a given charging duration will give different discharging durations. Equation (8) gives the charging time, while the discharging time is determined from Eq. (26). In this analysis, the charging time was fixed at 6 h. The discharge time varies with the source temperature, the geothermal fluid inlet and outlet temperature difference in the evaporator, and the sink temperature. Figure 6 shows the discharge temperature as a function of the source temperature for the different working fluids considered. The trend is the same as that of the net power ratio and COP. A higher discharge time means better performance of the system since the power input during charging and the power output during the discharge cycle are the same. The additional discharge time above the charging time is due to the additional thermal energy from the geothermal source. As such, when the discharge time is greater than the specified charging time, more electrical energy is delivered than what was used to charge the system. This corresponds to conditions that gave the net power ratio greater than 1 in Fig. 3.

Because Cyclopentane gave the best performance, the subsequent discussion considered this working fluid to further underpin the performance of the PTES system as other parameters change. Figure 7 shows the variation of the net power ratio with geothermal source temperature and the temperature difference between the inlet and exit of the geothermal fluid. As expected, a lower geothermal inlet and outlet temperature difference gives the highest net power ratios and COPs. This is because the average evaporator temperature is higher, requiring less power input to achieve the required condenser temperature. However, for constant power output, a lower geothermal inlet and outlet temperature difference means higher flowrates, as shown in Fig. 8. The flowrate ranges from 11 m^3/h to 1280 m^3/h. Higher flowrates are associated with higher source temperatures and lower geothermal fluid inlet and outlet temperature differences. First, such high flowrates might not be achievable in a single conventional geothermal system, requiring several

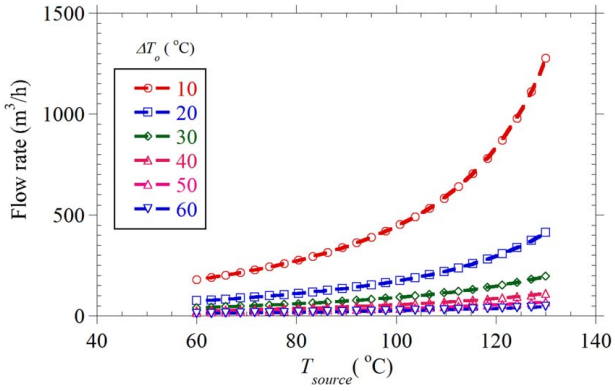

Fig. 8 Borehole heat exchanger flowrate with source temperature and geothermal fluid inlet and outlet temperature difference (ΔT_o) for cyclopentane with $T_{sink} = 20$ °C and a 1-MW system

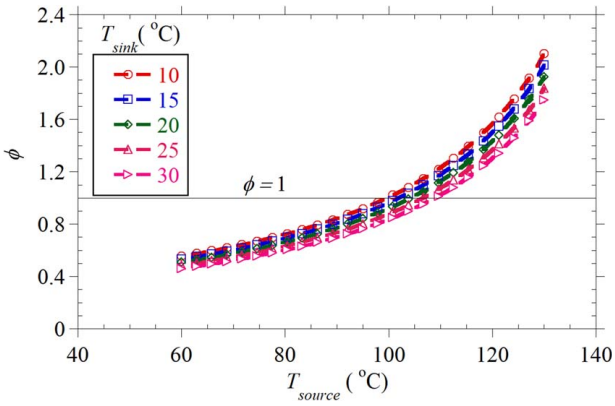

Fig. 9 Net power ratio as a function of source temperature and sink temperature for cyclopentane

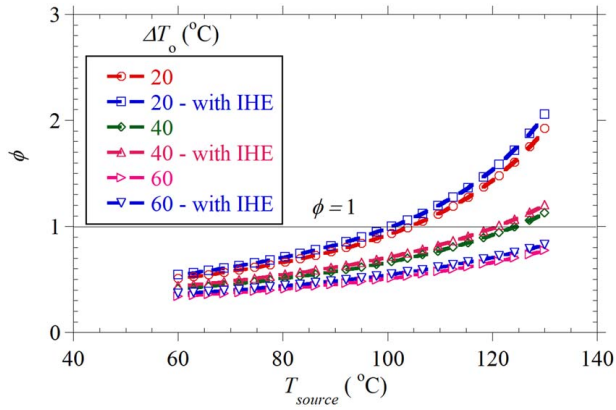

Fig. 10 Net power ratio with and without an IHE as a function of source temperature for cyclopentane with $T_{sink} = 20$ °C and a 1-MW system

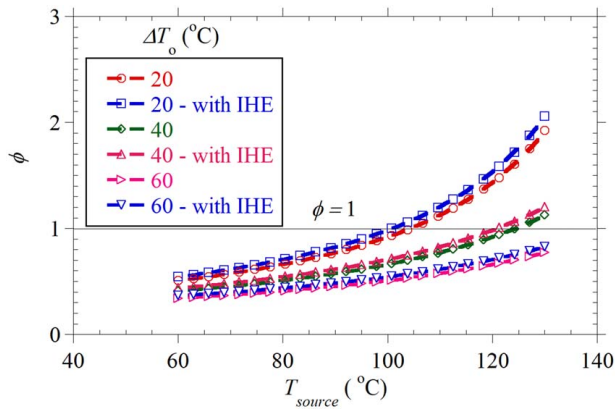

Fig. 11 Second law efficiency for the charging cycle as a function of the source temperature and geothermal fluid inlet and outlet temperature difference (ΔT_o) across the evaporator for cyclopentane with $T_{sink} = 20$ °C and a 1-MW system

wells to be drilled. For example, Alimonti et al. [19] demonstrated that 20 m^3/h flowrates were needed to ensure a 120 °C supply temperature with a 40 °C return temperature for a 6.1 km system. Second, such high flowrates will require large heat exchangers for minimum pressure drops.

Looking at the discharge cycle, since the source temperature is fixed by the melting temperature of the material in the thermal storage tank, the main parameter that affects the net power ratio is the sink temperature. Figure 9 shows the influence of the sink temperature on the net power ratio. The net power ratio slightly increases as the sink temperature reduces. This is in accordance with the variation in the efficiency of a heat engine cycle. Lowering the sink temperature increases the turbine work output without changing the heat supplied significantly. However, for air-cooled condensers and even water-cooled ones, the sink temperature is dictated by the ambient conditions and may be difficult to manipulate. In cold climates, the system will have the highest performance at the lowest ambient temperatures in winter.

To improve the performance of the PTES system, several modifications can be made. The simplest modification is recuperation by including an internal heat exchanger, as shown in Fig. 1(*b*). Figure 10 shows that including an internal heat exchanger improves the performance of the PTES system at each geothermal fluid inlet and outlet temperature difference considered. The range of parameters used in this study, including an internal heat exchanger, increases the net power ratio by as much as 8% depending on the source temperature, the working fluid used, and the geothermal fluid inlet and outlet temperature difference.

The second law efficiency is an indicator of how a system closely approaches a reversible and most efficient one. Figure 11 shows the second law efficiency of the charging cycle as a function of the source temperature and geothermal fluid inlet and outlet temperature difference. As shown, the second law efficiency increases as the source temperature increases and as the heat exchanger temperature difference reduces. This is in line with the first-law variation discussed earlier. A closer look at the system irreversibilities shows that the irreversibilities of the charging cycle increase as the geothermal fluid inlet and outlet temperature difference increase, thus lowering the exergetic or second-law efficiency.

Turbomachinery efficiencies can significantly influence the overall system performance. Thus far, results have been presented with compressor and turbine efficiencies at 90%, as presented in Table 2. Tables 3 and 4 show the influence of compressor isentropic efficiency on system performance for turbine efficiencies of 90% and 80%, respectively. As shown, as the compressor isentropic efficiency increases, the coefficient of performance of the heat pump becomes larger, and the net power ratio rises. This increase in the COP and net power ratio is a result of lower compressor power requirements at higher isentropic efficiencies. At a fixed compressor efficiency, the heat pump COP remains constant as the turbine efficiency changes since the charging and discharging processes do not occur simultaneously. However, the net power ratio increases since the power output of the turbine is largers at high values of the isentropic efficiencies. As the performance is better with larger compressor and turbine isentropic efficiencies, the discharge time increases. The system will generate 1 MW of electricity over a longer time with more efficient system components. This is in line with the variation of the net power ratio as earlier discussed.

Table 3 Performance at different compressor isentropic efficiencies with cyclopentane for $\Delta T_o = 20$ °C, $\Delta t_c = 6$ h, $T_{source} = 100$ °C, $T_{sink} = 20$ °C, and $\eta_t = 90\%$

Compressor isentropic efficiency, η_{ic}(%)	COP	Net power ratio, ϕ	Discharging time, Δt_d (hours)
70	4.06	0.76	4.71
75	4.28	0.80	4.96
80	4.50	0.85	5.21
85	4.72	0.89	5.67
90	4.94	0.93	5.72

Table 4 Performance at different compressor isentropic efficiencies with cyclopentane for $\Delta T_o = 20$ °C, $\Delta t_c = 6$ h, $T_{source} = 100$ °C, $T_{sink} = 20$ °C, and $\eta_t = 80\%$

Compressor isentropic efficiency, η_{ic}(%)	COP	Net power ratio, ϕ	Discharging time, Δt_d (hours)
70	4.06	0.68	4.18
75	4.28	0.72	4.41
80	4.50	0.75	4.63
85	4.72	0.79	4.86
90	4.94	0.82	5.08

The results highlight the performance of a geothermal integrated pumped thermal energy storage system with different environmentally friendly working fluids from a thermodynamic point of view. The study shows which working fluids give the best performance for the range of parameters considered. Thermodynamically, the results presented in this work show approximately how an actual system would operate. In an actual PTES system, a detailed analysis and sizing of the system components using heat transfer and fluid flow principles in addition to this thermodynamic analysis is essential.

7 Conclusion

In this study, a thermodynamic model of a geothermal integrated pumped thermal energy storage system was developed and used to evaluate overall system performance over a range of operating conditions and for different environmentally friendly working fluids. Geothermal source temperatures between 60 °C and 130 °C and a geothermal fluid inlet and outlet temperature difference between 10 °C and 60 °C were considered for the charging and discharging cycles of 1-MW power input and power output, respectively. The storage temperature of 133 °C was used, and PlusICE's A133 phase change material was used as the storage material. For the discharging cycle, sink temperatures between 15 °C and 30 °C were considered. The study shows that the net power ratio increases with increasing source temperatures. This is expected since the compressor would require less electrical power input to provide the necessary storage temperature since thermal energy from the geothermal source helps minimize the compressor temperature lift. Results further show that above some given source temperature and with a low-temperature difference of the geothermal fluid, net power ratios greater than 1 can be achieved. This means that such an energy storage system can give more than 100% of the electrical energy consumed during charging. Of the considered heat transfer fluids, cyclopentane gives the highest performance. This is because it has a significantly higher critical temperature than the melting temperature of the phase change material used and, thus, a higher latent heat of vaporization. Accordingly, performance increases with the latent heat of vaporization of the working fluid used, albeit with higher geothermal fluid flowrates. For cyclopentane, the net power ratio is greater than 1 at source temperatures greater than 100 °C and for a geothermal fluid inlet and outlet temperature difference of 20 °C, and source temperatures greater than 120 °C for a geothermal fluid inlet and outlet temperature difference of 40 °C. Geothermal fluid inlet and outlet temperature differences higher than 40 °C give net power ratios lower than 1 for the range of parameters considered.

Acknowledgment

The support received from the Schulich School of Engineering at the University of Calgary is duly acknowledged and appreciated.

Conflict of Interest

There are no conflicts of interest.

Data Availability Statement

The datasets generated and supporting the findings of this article are obtainable from the corresponding author upon reasonable request.

Nomenclature

h = enthalpy
s = entropy, J/kg K
v = specific volume, m^3/kg
L = latent heat, J/kg
Q = energy, J
T = temperature, K
$\dot{I}$ = irreversibility, W
$\dot{Q}$ = energy transfer rate, J/s
$\dot{W}$ = power output, W
c_{ps} = specific heat capacity of the thermal energy storage material, J/kg K
c_{pw} = specific heat capacity of heat exchanger fluid, J/kg K
m_s = mass of thermal energy storage tank material, kg
T_{in} = outlet temperature of the borehole heat exchanger/inlet into the evaporator, K
T_{out} = inlet temperature of the borehole heat exchanger/outlet from the evaporator, K
$\dot{m}_{r,c}$ = mass flowrate through the heat pump, kg/s
$\dot{m}_{r,d}$ = mass flowrate through the Rankine cycle, kg/s
$\dot{m}_w$ = mass flowate through the heat pump, kg/s
$\dot{S}_{gen}$ = entropy generation rate, W/K
Δt_c = charging time, h
Δt_d = discharging time, h
ΔT_o = geothermal fluid inlet and outlet temperature difference across the evaporator (T_{in}—T_{out}), K

Greek Symbols

η_{ic} = compressor isentropic efficiency
η_{th} = thermal efficiency
η_t = turbine isentropic efficiency
η_{II} = second law efficiency
ϕ = power-to-power ratio

Subscripts

c = compressor
$cond$ = condenser
ev = evaporator
exp = expansion device
f = final state
i = initial state
in = inlet
o = dead state condition
out = outlet

pump = pump
rev = reversible
r,c = refrigerant in the charging cycle
r,d = refrigerant in the discharging cycle
s = storage
sto,c = storage, charging
sto,d = storage, discharge
surr = surroundings
t = turbine
th = thermal

References

[1] World Energy Council, 2019, Energy Storage Monitor—Latest Trends in Energy Storage. Report No. FEL-100|2019. https://www.worldenergy.org/assets/downloads/ESM_Final_Report_05-Nov-2019.pdf, Accessed May 4, 2024.

[2] Olympios, A. V., McTigue, J. D., Farres-Antunez, P., Tafone, A., Romagnoli, A., Li, Y., Ding, Y., et al., 2020, "Progress and Prospects of Thermo-Mechanical Energy Storage—A Critical Review," Prog. Energy, **3**(2), p. 022001.

[3] Dumont, O., and Lemort, V., 2020, "Mapping of Performance of Pumped Thermal Energy Storage (Carnot Battery) Using Waste Heat Recovery," Energy, **211**, p. 118963.

[4] Steinmann, W. D., Bauer, D., Jockenhöfer, H., and Johnson, M., 2019, "Pumped Thermal Energy Storage (PTES) as Smart Sector-Coupling Technology for Heat and Electricity," Energy, **183**, pp. 185–190.

[5] Steinmann, W. D., 2014, "The CHEST (Compressed Heat Energy STorage) Concept for Facility Scale Thermo Mechanical Energy Storage," Energy, **69**, pp. 543–552.

[6] Parisi, S., Desai, N. B., and Haglind, F., 2024, "Techno-Economic Analysis of Using Reversible Turbomachinery for Pumped Thermal Energy Storage Systems," ASME J. Sol. Energy Eng., **146**(5), p. 051003.

[7] Jockenhöfer, H., Steinmann, W. D., and Bauer, D., 2018, "Detailed Numerical Investigation of a Pumped Thermal Energy Storage With Low Temperature Heat Integration," Energy, **145**, pp. 665–676.

[8] Frate, G. F., Antonelli, M., and Desideri, U., 2017, "A Novel Pumped Thermal Electricity Storage (PTES) System with Thermal Integration," Appl. Therm. Eng., **121**, pp. 1051–1058.

[9] Frate, G. F., Baccioli, A., Bernardini, L., and Ferrari, L., 2022, "Assessment of the Off-Design Performance of a Solar Thermally-Integrated Pumped-Thermal Energy Storage," Renew. Energy, **201**(Part I), pp. 636–650. .

[10] Weitzer, M., Müller, D., Steger, D., Charalampidis, A., Karellas, S., and Karl, J., 2022, "Organic Flash Cycles in Rankine-Based Carnot Batteries With Large Storage Temperature Spreads," Energy Convers. Manage., **255**, p. 115323.

[11] Tian, W., and Xi, H., 2022, "Comparative Analysis and Optimization of Pumped Thermal Energy Storage Systems Based on Different Power Cycles," Energy Convers. Manage., **259**, p. 115581.

[12] Steger, D., Regensburger, C., Eppinger, B., Will, S., Karl, J., and Schlücker, E., 2020, "Design Aspects of a Reversible Heat Pump—Organic Rankine Cycle Pilot Plant for Energy Storage," Energy, **208**, p. 118216..

[13] Zhao, Y., Song, J., Zhao, C., Zhao, Y., and Markides, C. N., 2022, "Thermodynamic Investigation of Latent-Heat Stores for Pumped-Thermal Energy Storage," J. Energy Storage, **55**(Part D), p. 105802.

[14] Eppinger, B., Zigan, L., Karl, J., and Will, S., 2020, "Pumped Thermal Energy Storage With Heat Pump-ORC-Systems: Comparison of Latent and Sensible Thermal Storages for Various Fluids," Appl. Energy, **280**, p. 115940.

[15] Niu, J., Wang, J., Liu, X., and Dong, L., 2023, "Optimal Integration of Solar Collectors to Carnot Battery System With Regenerators," Energy Convers. Manage., **277**, p. 116625.

[16] Steinmann, W.-D., 2022, "Pumped Thermal Energy Storage Based on High Temperature Steam Cycles," Encycl. Energy Storage, **2**, pp. 59–67.

[17] Caulk, R. A., and Tomac, I., 2017, "Reuse of Abandoned Oil and Gas Wells for Geothermal Energy Production," Renew. Energy, **112**, pp. 388–397.

[18] Mehmood, A., Yao, J., Fan, D., Bongole, K., Liu, J., and Zhang, X., 2019, "Potential for Heat Production by Retrofitting Abandoned Gas Wells into Geothermal Wells," PLoS One, **14**(8), p. e0220128..

[19] Alimonti, C., Berardi, D., Bocchetti, D., and Soldo Background, E., 2016, "Coupling of Energy Conversion Systems and Wellbore Heat Exchanger in a Depleted Oil Well," Geotherm. Energy, **4**(11), pp. 2–17..

[20] "PlusICE PCM Range". https://www.pcmproducts.net/,. Accessed January 5, 2023.

[21] "Regulation (EU) No. 517/2014 of the European Parliament and of the Council of 16 April 2014 on Fluorinated Greenhouse Gases and Repealing Regulation (EC) No 842/2006," Official J. Eur. Union, **L150**, pp. 195–230..

[22] "R1233ZD(E) | Product Information". https://www.agas.com/uk/products-and-services/refrigerants/r1233zd-e/, Accessed January 5, 2023].

[23] "EES: Engineering Equation Solver | F-Chart Software". https://fchartsoftware.com/ees/, Accessed May 3, 2024.